International Journal of Remote Sensing
Vol. 27, No. 5, 10 March 2006, 999–1014

Taylor & Francis
Taylor & Francis Group

Error sources on the land surface temperature retrieved from thermal infrared single channel remote sensing data

J. C. JIMÉNEZ-MUÑOZ and J. A. SOBRINO*

Global Change Unit, Department of Thermodynamics, Faculty of Physics, University of Valencia, Dr. Moliner 50, 46100, Burjassot, Spain

(*Received 30 April 2004; in final form 27 October 2004*)

In this paper, a theoretical study complementary to others given in the literature about the errors committed on the land surface temperature retrieved from the radiative transfer equation in the thermal infrared region by remote sensing techniques has been analysed. For this purpose, the MODTRAN 3.5 code has been used in order to simulate different conditions and evaluate the influence of several parameters on the land surface temperature accuracy: atmospheric correction, noise of the sensor, land surface emissivity, aerosols and other gaseous absorbers, angular effects, wavelength uncertainty, full-width half-maximum of the sensor and band-pass effects. The results show that the most important error source is due to atmospheric effects, which leads to an error on surface temperature between 0.2 K and 0.7 K, and land surface emissivity uncertainty, which leads to an error on surface temperature between 0.2 and 0.4 K. Hence, assuming typical uncertainties for remote sensing measurements, a total error for land surface temperature between 0.3 K and 0.8 K has been found, so it is difficult to achieve an accuracy lower than these values unless more accurate *in situ* values for emissivity and atmospheric parameters are available.

1. Introduction

The importance of land surface temperature for environmental studies has been pointed out by different authors (Barton 1992, Lagouarde *et al.* 1995, Qin and Karnieli 1999, Dash *et al.* 2002, Schmugge *et al.* 2002, etc.), so it is needed for water and energy budgets at the soil/atmosphere interface and evapotranspiration estimations among others. In order to retrieve the land surface temperature (hereinafter referred to as T_s or LST) from remote sensing data in the thermal infrared region, different techniques and algorithms have been applied, namely, single-channel equations, two-channel or split-window algorithms, dual-angle algorithms, etc. Most of them are based on approximations of the radiative transfer equation (RTE), which can be written in the thermal infrared region as

$$L_\lambda^{\text{at-sensor}} = \left\{ \varepsilon_\lambda B_\lambda(T_s) + (1-\varepsilon_\lambda) L_\lambda^{\text{atm}\downarrow} \right\} \tau_\lambda + L_\lambda^{\text{atm}\uparrow} \tag{1}$$

where ε_λ is the surface emissivity, $B(\lambda, T_s)$ is the radiance emitted by a blackbody at temperature T_s, $L_\lambda^{\text{atm}\downarrow}$ is the downwelling atmospheric radiance, in which the diffusive approximation for the downwelling atmospheric flux $F = \pi L_\lambda^{\text{atm}\downarrow}$ has been considered, τ_λ is the total transmission of the atmosphere (transmissivity) and

*Corresponding author. Email: sobrino@uv.es

International Journal of Remote Sensing
ISSN 0143-1161 print/ISSN 1366-5901 online © 2006 Taylor & Francis
http://www.tandf.co.uk/journals
DOI: 10.1080/01431160500075907

$L_\lambda^{\text{atm}\uparrow}$ is the upwelling atmospheric radiance. All these magnitudes also depend on the observation angle. However, it is also possible to obtain T_s directly from equation (1) by correcting the atmospheric effects and also the emissivity effect. Then, T_s can be calculated by inversion of the Planck's law.

The main goal of this paper is to obtain a quantitative estimation of the error associated with the T_s retrieved from the RTE (equation (1)) in order to contribute to other theoretical and experimental studies given in the literature, which provide errors committed on LST retrieved from other techniques (see, for example, Becker and Li 1990a, b, 1995, Li and Becker 1993, Prata 1993, 1994, Sobrino *et al.* 1993, 1994, 1996, Wan and Li 1997, etc.).

2. Sensitivity analysis

The purpose of this section is to carry out a sensitivity analysis of the RTE and its influence on the T_s. From equation (1), it is clear to notice that T_s depend on the atmospheric parameters (atmospheric transmissivity, τ_λ, upwelling atmospheric radiance or path radiance, $L_\lambda^{\text{atm}\uparrow}$, and downwelling atmospheric radiance, $L_\lambda^{\text{atm}\downarrow}$), the at-sensor radiance ($L_\lambda^{\text{at-sensor}}$) and the land surface emissivity (ε_λ). The error on the T_s due to the uncertainties of these parameters is analysed in the following sections. For this purpose, the MODTRAN 3.5 (Abreu and Anderson 1996) code has been used in order to simulate different conditions and evaluate the influence of the parameters above-mentioned on the LST accuracy.

In order to focus the study, the midlatitude summer (MLS) atmosphere has been chosen from the MODTRAN standard atmospheres. In figure 1 the transmissivity spectrum for the MLS atmosphere is represented. The main atmospheric absorbers are also indicated. The following well-known regions can be observed: in the range 8–9 μm an increasing tendency with strong absorptions is observed. The absorption for this range is due mainly to the atmospheric water vapour content and secondly to other atmospheric absorbers as N_2O, CO^+_2 and CH_4. In the range 9–10 μm a strong absorption is observed. This absorption is mainly due to the ozone and it is

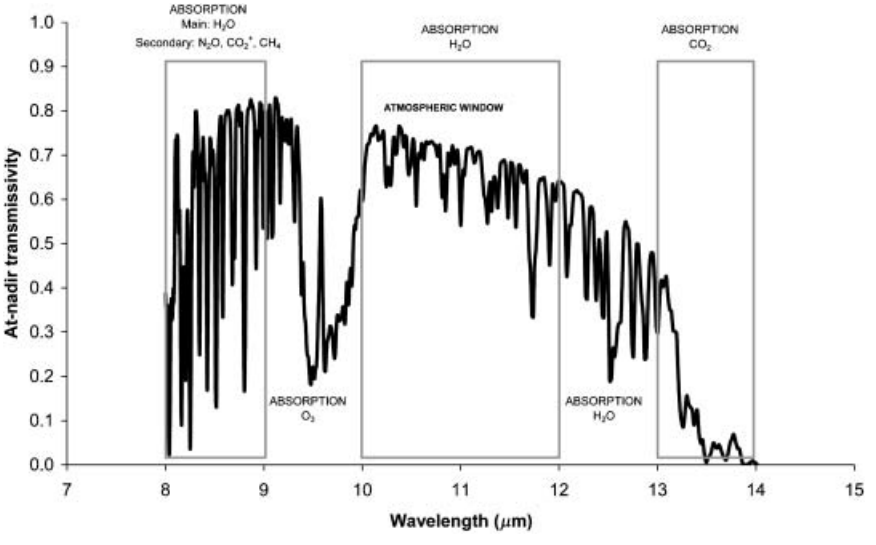

Figure 1. Transmissivity spectrum for the midlatitude summer atmosphere.

centred more or less at 9.5 μm. In the range 10–12 μm a slightly descending tendency is observed, but high atmospheric transmissivity values are obtained. The absorption peaks are weaker than the ones observed in the 8–9 μm, so this region is the most used in thermal infrared remote sensing and it is called 'atmospheric window'. In the region 12–13 μm the transmissivity values are lower than the ones obtained in 10–12 μm, and the main absorption is due to the atmospheric water vapour content. Finally, in the range 13–14 μm, a strong absorption due to the CO_2 is observed. In this region the atmosphere is practically opaque to the thermal radiance. It should be noted that the results shown in the next sections have been spectrally obtained for the atmospheric window region, between 10 and 12 μm (in steps of 1 cm^{-1}), and then a mean value with the standard deviation and the r.m.s. deviation has been calculated. This option has been chosen instead of using a particular filter function in order to obtain general results and not particularized for any thermal sensor. Anyway, a mean value is equivalent to a square filter function from 10 to 12 μm. Unless otherwise stated, the MODTRAN 3.5 code has been executed in thermal radiance mode for a MLS atmosphere, in clear-sky conditions, with a view angle of nadir, considering an emissivity value of 0.98 and a surface temperature of 300 K.

2.1 *Atmospheric correction*

In order to obtain accurate land surface temperature values, atmospheric effects must be removed. The parameters involved in the atmospheric correction are the atmospheric transmissivity (τ_λ), the upwelling atmospheric radiance or path radiance ($L_\lambda^{\text{atm}\uparrow}$) and the downwelling atmospheric radiance ($L_\lambda^{\text{atm}\downarrow}$). These parameters are correlated and they depend mainly on the atmospheric water vapour content (w). Hence, when the atmospheric water vapour increases, the atmospheric transmissivity decreases and the upwelling and downwelling radiances increase. So in order to evaluate the error committed on T_s due to atmospheric effects, $e_w(T_s)$, the following equation has been considered:

$$e_w(T_s) = \left(\frac{\partial T_s}{\partial w}\right) e(w) = \left[\left(\frac{\partial B_\lambda(T_s)}{\partial w}\right)\left(\frac{\partial T_s}{\partial B_\lambda(T_s)}\right)\right] e(w) \equiv \delta_w^B \delta_B^T e(w) \tag{2}$$

where $e(w)$ is the error on water vapour. Assuming that the atmospheric parameters depend on the water vapour content, the term Δ_w^B can be obtained according to the following equation:

$$\delta_w^B \equiv \left|\frac{\partial B_\lambda(T_s)}{\partial w}\right| = \left|\left[\frac{\partial B_\lambda(T_s)}{\partial \tau_\lambda}\frac{\partial \tau_\lambda}{\partial w} + \frac{\partial B_\lambda(T_s)}{\partial L_\lambda^{\text{atm}\uparrow}}\frac{\partial L_\lambda^{\text{atm}\uparrow}}{\partial w} + \frac{\partial B_\lambda(T_s)}{\partial L_\lambda^{\text{atm}\downarrow}}\frac{\partial L_\lambda^{\text{atm}\downarrow}}{\partial w}\right]\right| \tag{3}$$

whereas the term δ_B^T is obtained by deriving the Planck's function and is given by:

$$\delta_B^T \equiv \left|\frac{\partial T_s}{\partial B_\lambda(T_s)}\right| = \left|\left[\frac{c_{2\lambda}c_{1\lambda}}{c_{1\lambda}B_\lambda(T_s) + B_\lambda^2(T_s)}\right]\left[\ln^2\left(\frac{c_{1\lambda}}{B_\lambda(T_s)} + 1\right)\right]^{-1}\right| \tag{4}$$

with $c_{1\lambda} = 1.19104 \cdot 10^8\, \lambda^{-5}$ and $c_{2\lambda} = 14387.7\, \lambda^{-1}$. In the previous equation radiance is given in watts m^{-2} μm^{-1} sr^{-1}, temperature in K and wavelength in μm. In order to apply the equation (3), the expression for $B_\lambda(T_s)$ as a function of the atmospheric parameters is needed, which can be easily obtained from equation (1), and also the dependence of the atmospheric parameters with the atmospheric water vapour

content. For this purpose, a simulation using MODTRAN 3.5 and a set of 60 radiosoundings extracted from the TIROS Operational Vertical Sounder (TOVS) Initial Guess Retrieval (TIGR) database (Scott and Chedin 1981) has been carried out. The simulation procedure performed for the 10–12 μm square filter shows the following results:

$$\langle \tau \rangle_{10-12\mu m} = -0.1514\ w + 1.028 (r = 0.996,\ \sigma = 0.02) \tag{5a}$$

$$\langle L^{\text{atm}\uparrow} \rangle_{10-12\mu m} = 0.7194\ w^{1.358} (r = 0.997,\ \sigma = 0.1) \tag{5b}$$

$$\langle L^{\text{atm}\downarrow} \rangle_{10-12\mu m} = 1.161\ w^{1.228} (r = 0.996,\ \sigma = 0.1) \tag{5c}$$

where r is the correlation coefficient and σ the standard error of estimate. Hence, from equation (3) it is easy to obtain the final expression for δ_w^B:

$$\delta_w^B \equiv \left| \frac{\partial B_\lambda(T_s)}{\partial w} \right| = \left| \frac{-0.1514 \left(L_\lambda^{atm\uparrow} - L_\lambda^{at\text{-}sensor} \right)}{\varepsilon_\lambda \tau_\lambda^2} - \frac{0.9769 w^{0.358}}{\varepsilon_\lambda \tau_\lambda} + \left(1 - \frac{1}{\varepsilon_\lambda} \right) \left(1.4257 w^{0.228} \right) \right| \tag{6}$$

Finally, from equations (2), (4) and (6) it is possible to obtain the values shown in figure 2, in which the ratio between the error on T_s, $e(T_s)$, and the error on water vapour, $e(w)$, versus the water vapour is graphed. It should be noted that greater errors are committed for low and high atmospheric water vapour contents, with a minimum error located at 3 g cm^{-2}. Hence, assuming a typical water vapour uncertainty of 0.5 g cm^{-2} (Sobrino *et al.* 2002), an error on T_s of 2.6 K, 1.1 K, 0.3 K and 1 K is obtained when the total atmospheric water vapour content is 1 g cm^{-2},

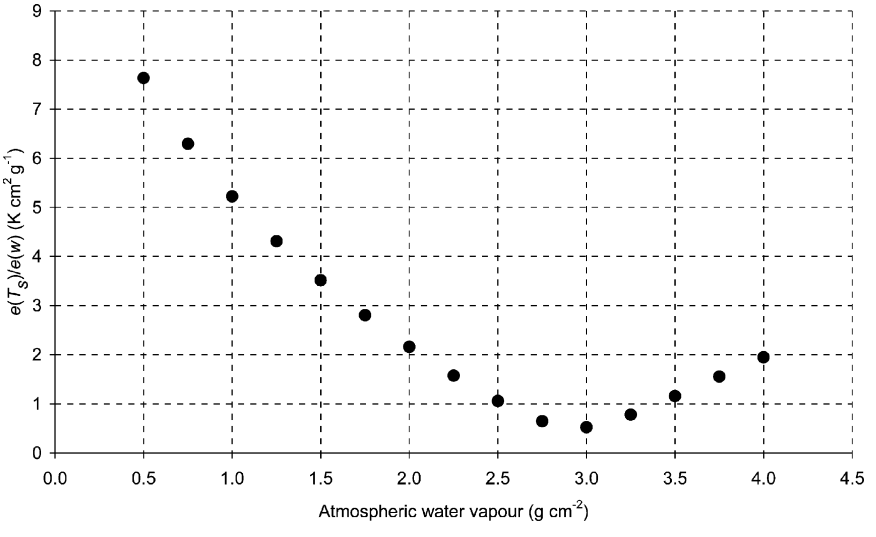

Figure 2. Ratio between the error on T_s and the error on atmospheric water vapour versus the atmospheric water vapour.

$2\,g\,cm^{-2}$, $3\,g\,cm^{-2}$ and $4\,g\,cm^{-2}$, respectively. Taking into account the standard atmospheric water vapour content for a MLS atmosphere, $2.36\,g\,cm^{-2}$, an error on T_s of 0.7 K is obtained. When w is measured *in situ* low errors can be obtained, as for example $0.15\,g\,cm^{-2}$ (Estellés, personal communication 2004). In this case, the previous errors are reduced to 0.8 K, 0.3 K, 0.08 K and 0.3 K, respectively, and for the MLS atmosphere an error of 0.2 K is obtained.

Although the atmospheric parameters are correlated and depend on w, sometimes it is interesting to analyse the effect of each parameter independently, as for example when *in situ* measurements with filed radiometers are made. In this case, the at-surface radiance given by the term $\varepsilon_\lambda B_\lambda(T_s)+(1-\varepsilon_\lambda)L_\lambda^{\text{atm}\downarrow}$ is measured, so only the downwelling radiance must be known. The error on T_s due to the uncertainty of the $L_\lambda^{\text{atm}\downarrow}$ can be obtained from the following equation:

$$e_{L\text{atm}\downarrow}(T_s)=\delta^B_{L\text{atm}\downarrow}\delta^T_B e\left(L_\lambda^{\text{atm}\downarrow}\right) \tag{7}$$

where

$$\delta^B_{L\text{atm}\downarrow}\equiv\left|\frac{\partial B_\lambda(T_s)}{\partial L_\lambda^{\text{atm}\downarrow}}\right|=\left|1-\frac{1}{\varepsilon_\lambda}\right| \tag{8}$$

Figure 3 shows the error on T_s depending on the land surface emissivity value considered. For emissivity values between 0.8 and 1, the error on T_s is less than 0.1 K when the uncertainty on the downward radiance is 1% and less than 0.7 K when the uncertainty is 10%. Moreover, the error on T_s also depends on the surface temperature value considered. Anyway, this dependence is negligible. As an example and assuming an uncertainty of 10% on the downward radiance, the error on T_s changes from 0.07 K to 0.04 K when the T_s value changes from 273 K to 373 K (assuming in this case an emissivity of 0.98). In order to obtain a global view for both dependences, figure 4 shows the error on T_s depending on the emissivity and

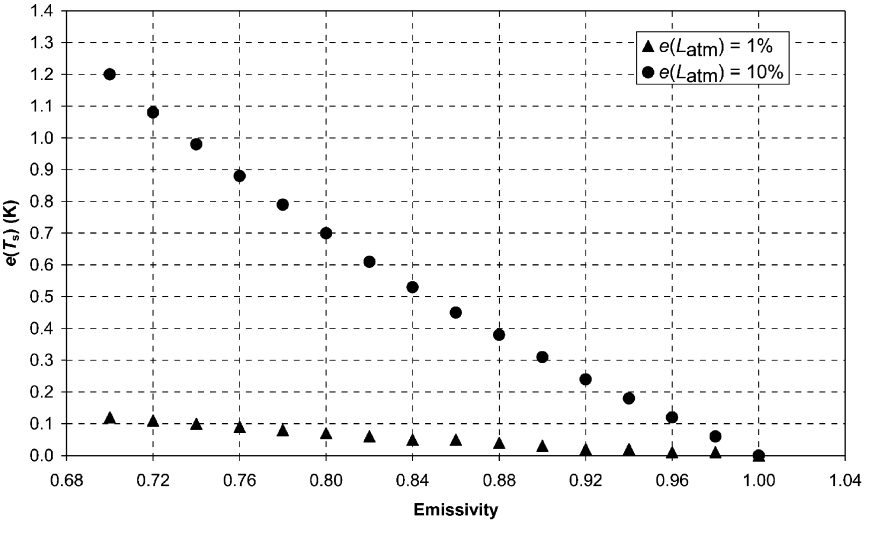

Figure 3. Error on land surface temperature (K) due to the uncertainty on the downward radiance depending on the land surface emissivity value considered.

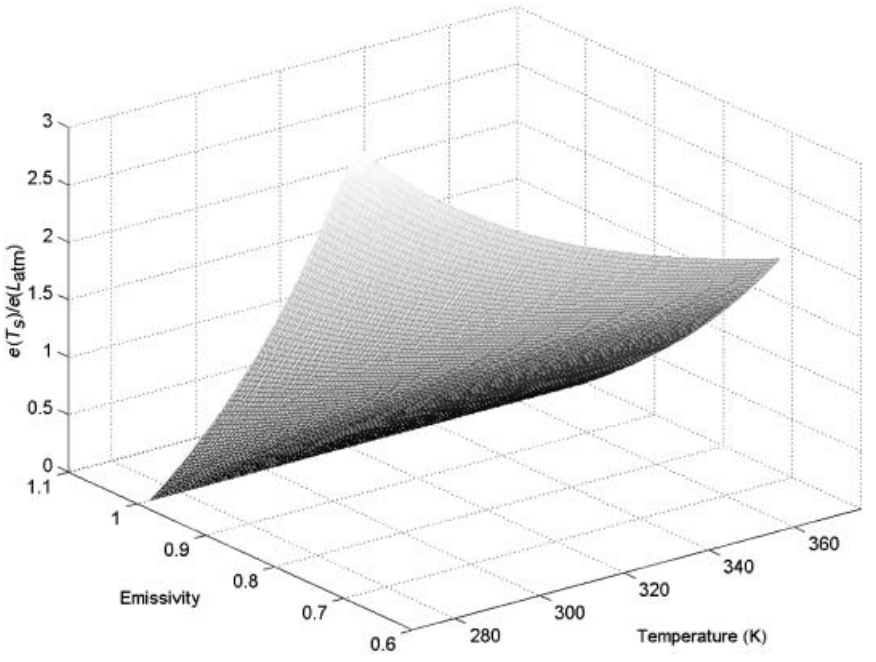

Figure 4. Error on T_s and error on downward radiance ratio depending on the land surface emissivity and temperature values. A fixed wavelength of 11 μm has been considered.

temperature values for a fixed wavelength of 11 μm. The smaller the emissivity and temperature, the greater the temperature retrieval error.

2.2 *Noise equivalent delta error*

The radiance measured by a sensor onboard a satellite is affected by an inherent uncertainty due to electronic devices involved in the construction of the sensor. The error on T_s due to the at-sensor radiance uncertainty is given by

$$e_{L\text{sensor}}(T_s) = \delta^B_{L\text{sensor}} \delta^T_B e\left(L_\lambda^{\text{at-sensor}}\right) \tag{9}$$

where

$$\delta^B_{L\text{sensor}} \equiv \left| \frac{\partial B_\lambda(T_s)}{\partial L_\lambda^{\text{at-sensor}}} \right| = \frac{1}{\varepsilon_\lambda \tau_\lambda} \tag{10}$$

The results obtained with these equations show an error on T_s of 0.1 K, 1 K and 10 K for at-sensor radiance uncertainties of 0.1%, 1% and 10%, respectively. Equation (4) can be used to estimate the equivalence between an uncertainty on radiance and an uncertainty on temperature. As an example, an uncertainty of 0.1 K in temperature leads to an error of 0.15% on radiance, whereas an uncertainty of 0.3 K in temperature leads to an error of 0.44% on radiance when the wavelength is 11 μm and the surface temperature is 300 K. Most of the thermal sensors have noise errors between 0.1 K and 0.3 K, as AVHRR (Advanced Very High Resolution Radiometer), ASTER (Advanced Spaceborne Thermal Emission and Reflection radiometer), etc., so it is expected to have uncertainties on the at-sensor radiances

between 0.1% and 0.5%. According to these results, the error on T_s due to the NEΔT is comprised between 0.1 K and 0.5 K. This error is practically negligible for thermal sensors with very low noise errors, as the AATSR (Advanced Along Track Scanning Radiometer), with a NEΔT of 0.05 K.

2.3 *Land surface emissivity*

The influence of the land surface emissivity uncertainty on T_s can be estimated as in the previous cases according to

$$e_{\varepsilon}(T_s) = \delta_{\varepsilon}^{B} \delta_{B}^{T} e(\varepsilon_{\lambda}) \tag{11}$$

where

$$\delta_{\varepsilon}^{B} \equiv \left| \frac{\partial B_{\lambda}(T_s)}{\partial \varepsilon_{\lambda}} \right| = \left| \frac{1}{\varepsilon_{\lambda}^{2}} \left[\left(\frac{L_{\lambda}^{\text{atm}\uparrow} - L_{\lambda}^{\text{at-sensor}}}{\tau_{\lambda}} \right) + L_{\lambda}^{\text{atm}\downarrow} \right] \right| \tag{12}$$

Here, errors on T_s of 0.04 K, 0.4 K and 4 K are obtained when the uncertainty on the land surface emissivity is 0.1%, 1% and 10%, respectively. The land surface emissivity is the main error source on the LST retrieval (excluding external factors as a worse calibration of the sensor). Land surface emissivity is typically retrieved from remote sensing data with an accuracy of 1% (Gillespie *et al.* 1998, Sobrino *et al.* 2002, etc.), which leads to an error of 0.4 K on the LST retrieval. Emissivity can be measured *in situ* with an accuracy of 0.5% (Sobrino and Caselles 1993, Nerry *et al.* 1998), which reduces the error on LST to 0.2 K. It should be noted that the error on T_s depends on the emissivity value chosen (and also on the LST value). The results mentioned have been obtained assuming an emissivity value of 0.98 and T_s=300 K. Figure 5 shows the error on T_s for different emissivity values when the uncertainty on emissivity is 0.01 and T_s=300 K. Most natural surfaces have emissivity values

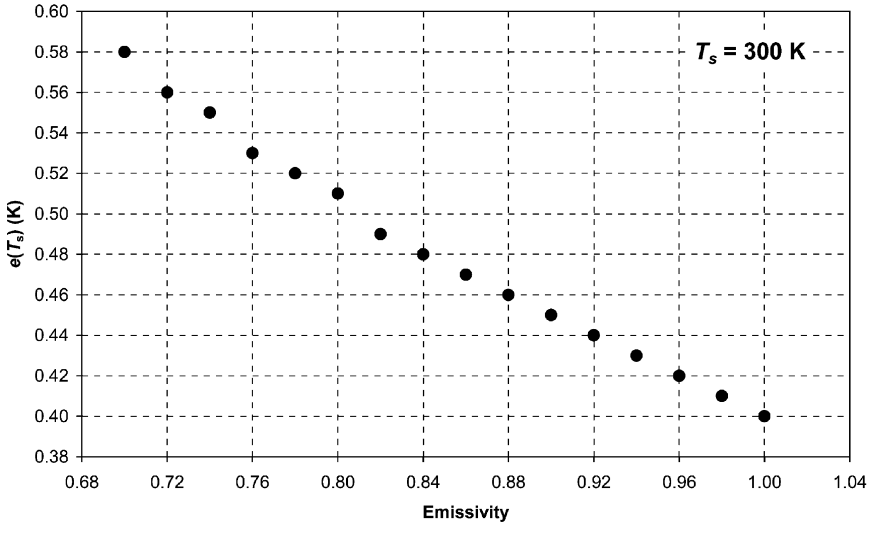

Figure 5. Error on land surface temperature (T_s) depending on the land surface emissivity value. An uncertainty on the emissivity of 0.01 and a value of 300 K for land surface temperature have been assumed.

between 0.8 and 1 in the region 10–12 μm, so errors on T_s between 0.4 and 0.5 K will be expected independently on the emissivity value. In this case, the error dependence on the surface temperature has been also analysed. Hence, when T_s changes from 273 K to 373 K, the error changes between 0.2 K and 0.9 K assuming a fixed emissivity value of 0.98. Both dependences, on temperature and emissivity, are given in figure 6. The T_s error rises with increasing surface temperature and emissivity (for a fixed wavelength of 11 μm).

3. Effects of aerosols and other gaseous absorbers

Although to retrieve the LST it is usual to assume clear-sky conditions and no aerosols attenuation, the aerosols effect in the thermal infrared region is not always negligible. Table 1 shows the differences between atmospheric transmissivity when the MODTRAN standard aerosols models are considered with respect to an

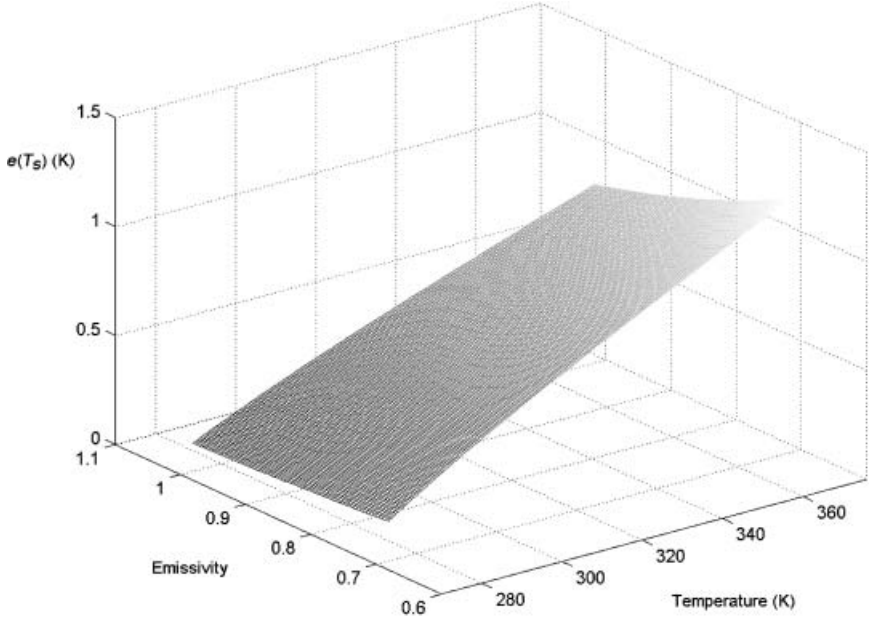

Figure 6. Error on land surface temperature (T_s) depending on the land surface emissivity and temperature values.

Table 1. Differences between atmospheric transmissivity without including the aerosols effect and considering different types of aerosols extinction in the region 10–12 μm.

Aerosols model	$\tau_{\text{aerosol}} - \tau_{\text{no-aerosol}}$ (%)
Rural extinction, visibility=23 km	1.9
Rural extinction, visibility=5 km	8.1
Navy maritime extinction	0.9
Maritime extinction, visibility=23 km	2.4
Urban extinction, visibility=5 km	9.1
Tropospheric extinction, visibility=50 km	0.2
Radiative fog extinction, visibility=0.5 km	90.7
Desert extinction	0.4

atmosphere without aerosols content. The lowest difference in transmissivity is 0.2%, which corresponds to the tropospheric extinction with a default visibility of 50 km. In this case the aerosols effect is negligible and correction is not needed. However, there are great differences between the transmissivity spectrum for an atmosphere with no aerosols content and an atmosphere with fog extinction and a default visibility of 0.5 km. It is clear that in this case the acquisition of a satellite image for remote sensing studies has no sense.

In addition to the aerosols effect, other gaseous absorbers also have an influence on the LST retrieved. As is well known, in the thermal infrared region the main atmospheric absorber is the water vapour. The CO_2 and CH_4 are secondary absorbers, and their variation has not a relevant importance on the LST value. As an example, let us consider the variation on the CO_2 concentration. The MODTRAN 3.5 code establishes a default value of CO_2 of 330 ppmv. However, values recommended in 1995 are 355–360 ppmv. Table 2 shows the values for the atmospheric parameters and LST when the CO_2 concentration varies from 330 ppmv to 380 ppmv. When the LST values obtained are analysed, an increase of around 0.004 K is observed when the CO_2 concentration increases 5 ppmv. A total difference of 0.04 K on LST is obtained when the CO_2 concentration in changed from 330 ppmv to 380 ppmv, so this effect on LST is negligible.

4. Angular effects

LST retrieved assuming at-nadir view angle is not always accurate enough, so most sensors have field of views (FOV) higher than 50° (for example, AVHRR and AATSR). In order to analyse the angular effects, simulations with the MODTRAN 3.5 code have been carried out for seven view angles, from 0° to 60° by steps of 10°. As an example, figure 7 illustrates the atmospheric transmissivity differences in % between the values obtained for these angles and the ones obtained for a nadir view. The graph shows differences lower than 1% for a view angle of 10° and differences higher than 2% for a view angle of 20°, whereas differences higher than 30% are obtained for view angles of 60°. In order to analyse the error committed on T_s when at-nadir view is assumed along all the FOV of the sensor, the effect of the view angle on water vapour values will be studied. As is well known, the relation between the atmospheric water vapour at certain view angle (θ) and the one at nadir view (0°) is

Table 2. Effect of the CO_2 concentration on the atmospheric parameters and on the retrieved land surface temperature from equation (1) at 11 μm.

CO_2 (ppmv)	τ	$L^{\text{atm}\uparrow}$ ($\text{W m}^{-2}\,\text{sr}^{-1}\,\mu\text{m}^{-1}$)	$L^{\text{atm}\downarrow}$ ($\text{W m}^{-2}\,\text{sr}^{-1}\,\mu\text{m}^{-1}$)	T_s(K)
330	0.6706	2.5508	3.7733	300.000
335	0.6705	2.5514	3.7742	300.004
340	0.6704	2.5520	3.7751	300.009
345	0.6703	2.5526	3.7760	300.013
350	0.6702	2.5531	3.7769	300.018
355	0.6701	2.5537	3.7778	300.022
360	0.6700	2.5543	3.7787	300.026
365	0.6699	2.5548	3.7796	300.031
370	0.6698	2.5554	3.7804	300.035
375	0.6697	2.5560	3.7813	300.040
380	0.6696	2.5565	3.7822	300.044

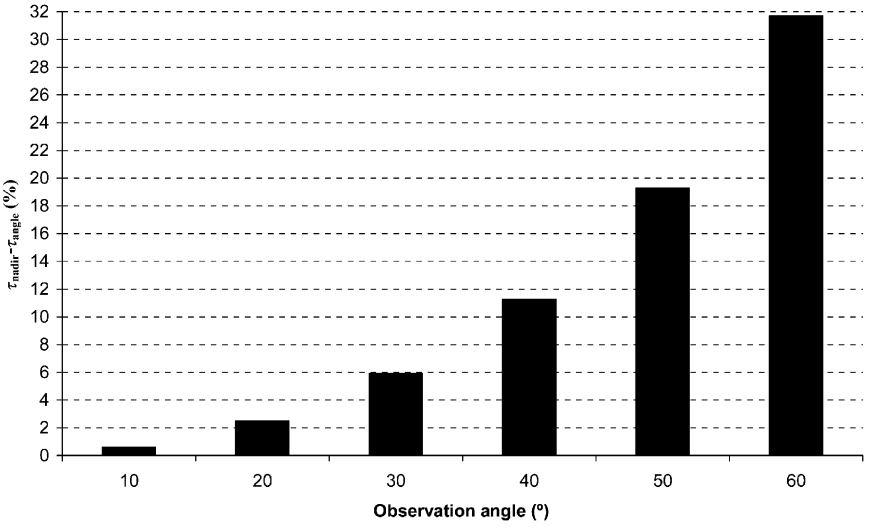

Figure 7. Angular effect on transmissivity (10–12 μm).

given by:

$$w(\theta)=\frac{w(0^\circ)}{\cos\theta}\Rightarrow\Delta w=w(0^\circ)\left(\frac{1}{\cos\theta}-1\right) \tag{13}$$

where Δw is the difference between $w(\theta)$ and $w(0^\circ)$. Assuming the difference Δw as the error on w, $e(w)$, due to angular effects and taking into account equations (2), (4) and (6), it is possible to obtain the following equation:

$$e(T_s)=kw(0^\circ)\left(\frac{1}{\cos\theta}-1\right) \tag{14}$$

where $e(T_s)$ is the error on T_s due to angular effects and k is a magnitude which depends on several parameters as wavelength, temperature, emissivity, etc. In fact, k is given by $\delta_w^B\delta_B^T$ (see §3.1). For the conditions considered in the paper (MLS atmosphere, $T_s=300$ K, $\varepsilon=0.98$ and 10–12 μm), a value of $k=4.0497$ is obtained. The results obtained according to equation (14) are represented in figure 8, in which a typical value of $w=2.36\,\mathrm{g\,cm^{-2}}$ for an MLS atmosphere has been considered. This figure shows that for view angles lower than 25°, the error on T_s is lower than 1 K. As an example, for a view angle of 55°, the error on T_s is higher than 7 K. For the moment, homogeneous and flat surfaces have been considered. However, angular effects can be also noticed for heterogeneous and rough surfaces pixels (Sobrino *et al.* 1990), which is a more complex situation and will not be treated in this paper.

It should be mentioned that the errors due to the land surface emissivity angular dependence must be also taken into account. Most natural surfaces show emissivity differences between nadir and certain angle view higher or equal to 0.01 for view angles higher than 30° (Sobrino and Cuenca 1999). These differences will lead to errors on T_s equal to or higher than 0.4 K. As an example, for a view angle of 55° the emissivity difference with respect to the nadir view for water is 0.04, which leads to an error on T_s higher than 1 K (see §3.3).

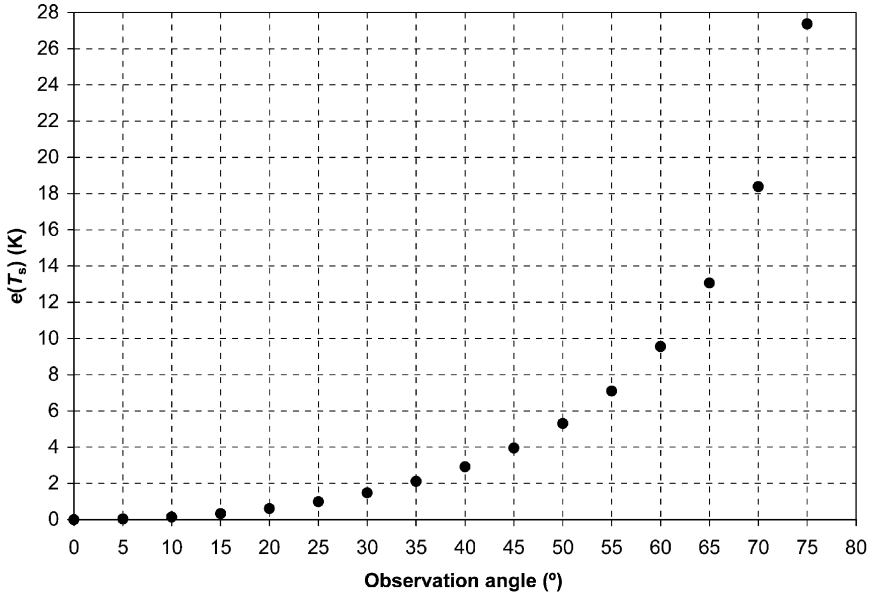

Figure 8. Error on land surface temperature (T_s) when angular effects are not considered, i.e. when at-nadir values are assumed for the whole field of view (FOV) of the sensor, versus the view angle.

5. Wavelength uncertainty

In order to obtain LST from the radiative transfer equation, it is necessary to invert the Planck's law. For this purpose, a value of wavelength is required. The goal of this section is to analyse the error on LST obtained with the Planck's law due to the wavelength uncertainty. This error can be calculated using the following equations:

$$e_\lambda(T_s) = \delta_\lambda^T e(\lambda) \tag{15}$$

where δ_λ^T is given by

$$\delta_\lambda^T \equiv \left|\frac{\partial T_s}{\partial \lambda}\right| = \left|\frac{g_1 g_2 - g_3 g_4}{g_2^2}\right| \tag{16}$$

and the functions g_i (i=1,4) are given by

$$g_1 \equiv -\frac{c_2}{\lambda^2} \tag{17a}$$

$$g_2 \equiv \ln\left[\left(\frac{c_1}{\lambda^5 B}\right) + 1\right] \tag{17b}$$

$$g_3 \equiv \frac{-5c_1}{\lambda c_1 + B\lambda^6} \tag{17c}$$

$$g_4 \equiv \frac{c_2}{\lambda} \tag{17d}$$

with B the radiance emitted by a blackbody at temperature T_s, $c_1 = 1.19104 \cdot 10^8\,\mathrm{W}\,\mu\mathrm{m}^4\,\mathrm{m}^{-2}\,\mathrm{sr}^{-1}$ and $c_2 = 14387.7\,\mu\mathrm{m}$ K (λ and T_s are given in μm and K, respectively). Assuming an uncertainty on the wavelength of 0.1 μm and different surface temperatures, the results shown in figure 9 are obtained. The following ideas can be extracted from this graph.

i) The error on T_s decreases when the wavelength increases until a certain inflexion point, from which the error on T_s increases when the wavelength increases. This inflexion point is 10.6 μm, 9.7 μm and 9.0 μm for a T_s value of 273 K, 300 K and 323 K, respectively. Therefore, the wavelength value of this inflexion point decreases when the T_s increases.
ii) At the inflexion point, the error on T_s is negligible.
iii) As an example, at 11 μm a wavelength uncertainty of 0.1 μm produces an error on T_s of 0.09 K, 0.4 K and 0.6 K when T_s is 273 K, 300 K and 323 K, respectively.

These results illustrate the importance of choosing an appropriate wavelength in order to invert the Planck's law. Normally, there are two options: (1) the central wavelength or (2) the effective wavelength, according to the channel filter function of the sensor. These two values of wavelength can differ significantly, so errors on T_s higher than a half of a degree can be committed.

6. Bandpass and FWHM effects

The sensor onboard a satellite measures with finite banded radiometers having a characteristic response function. This fact introduces an error on the LST retrieved. If $B_\lambda(T_s)$ is the radiance emitted by a blackbody at temperature T_s and $f(\lambda)$ is the response function or filter functions of the sensor, the radiance measured by the sensor $<B_\lambda(T_s)>_{\mathrm{sensor}}$ is given by

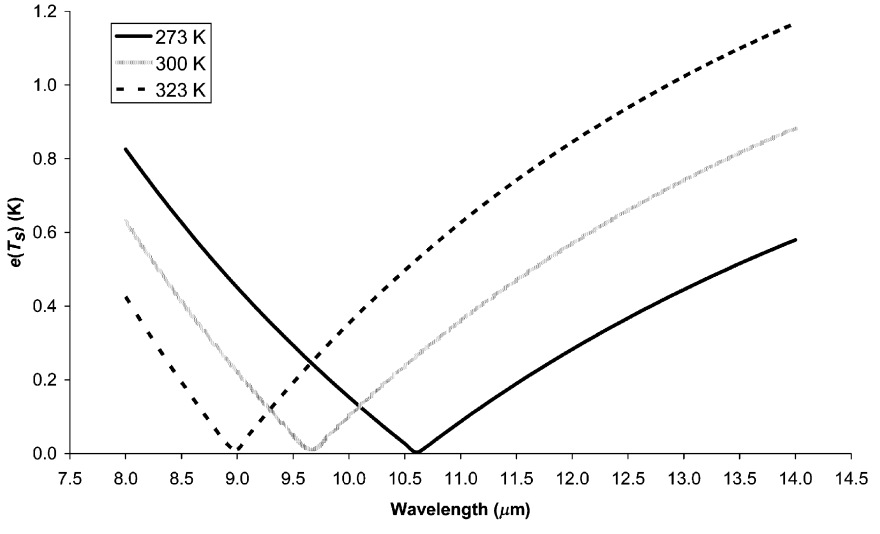

Figure 9. Error on land surface temperature due to an uncertainty of 0.1 μm on the wavelength.

$$\langle B_\lambda(T_s)\rangle_{\text{sensor}} = \frac{\int B_\lambda(T_s) f(\lambda)\mathrm{d}\lambda}{\int f(\lambda)\mathrm{d}\lambda} \tag{18}$$

T_s is obtained from $<B_\lambda(T_s)>_{\text{sensor}}$ by inversion of the Planck's law using the effective wavelength calculated with the following expression:

$$\lambda_{\text{effective}} = \frac{\int \lambda f(\lambda)\mathrm{d}\lambda}{f(\lambda)\mathrm{d}\lambda} \tag{19}$$

To analyse the error committed on this process, let us consider a blackbody at a temperature of 300 K and an ideal filter function similar to a Gaussian with a full-width half-maximum (FWHM) value of 1 μm and centred at 11 μm (Jiménez-Muñoz and Sobrino 2003). When the radiance measured by the radiometer is calculated using equation (18) and T_s is retrieved using the effective wavelength given by equation (19), a value of 299.85 K is obtained. This result shows a difference of 0.15 K with regard to the real value of T_s (300 K). This difference depends on the T_s value. So, if we choose a value of 273 K and 323 K for T_s, a difference of 0.17 K and 0.12 K is obtained, respectively. These differences also depend on the wavelength considered and on the FWHM of the filter function, as is shown in table 3. When the FWHM increases, the error on the T_s increase also, while when the wavelength increases the error decreases.

It should be noted that this error can be sometimes avoided if the filter functions of the sensor are known. However, in some cases the filter functions are not available or, even if they are available, most authors use the effective wavelength in order to simplify the calculus. Anyway, this effect cannot be avoided when at-sensor values are used. More details about bandpass effects can be found in Richter and Coll (2002).

7. Total error on LST

Once the error sources on the LST retrieval from thermal infrared remote sensing have been analysed, we are in the position of estimating a total error. For this purpose, the following equation is used:

$$e(T_s) = \sqrt{\sum_i e_i^2(T_s)} \tag{20}$$

where $e_i(T_s)$ is the error on T_s due to the different factors discussed: transmissivity,

Table 3. Error on land surface temperature (in K) due to bandpass effects (T_s=300 K).

λ (μm)	FWHM=0.5 (μm)	FWHM=1 (μm)	FWHM=2 (μm)
8	0.09	0.37	1.45
9	0.08	0.30	1.21
10	0.06	0.22	0.90
11	0.04	0.15	0.60
12	0.02	0.08	0.34
13	0.01	0.03	0.12
14	0.00	0.02	0.05

upward and downward radiances, emissivity, angular effects, etc. In order to obtain a value for $e(T_s)$ let us consider a typical situation: surface temperature 300 K, emissivity 0.98, wavelength 11 μm, FWHM 1 μm, a midlatitude summer atmosphere ($w=2.36\,\mathrm{g\,cm^{-2}}$), clear sky conditions, no aerosols and nadir view. Assuming an uncertainty on water vapour of $0.15\,\mathrm{g\,cm^{-2}}$, a NE$\Delta$T of 0.1 K, an uncertainty of 1% on emissivity and an uncertainty of 0.1 μm on wavelength, the application of equation (15) leads to an error on T_s of 0.6 K. If a NEΔT of 0.3 K is considered, then the error on T_s is 0.8 K. When an uncertainty of $0.5\,\mathrm{g\,cm^{-2}}$ instead of $0.15\,\mathrm{g\,cm^{-2}}$ for the atmospheric water vapour is considered, the error on T_s is 0.9 K and 1 K for NEΔT of 0.1 K and 0.3 K, respectively. Taking into account the error on T_s only due to the emissivity and water vapour uncertainties, values of 0.5 K and 0.8 K are obtained assuming an uncertainty on the emissivity of 1% and $0.15\,\mathrm{g\,cm^{-2}}$ and $0.5\,\mathrm{g\,cm^{-2}}$ for water vapour, respectively. When an uncertainty on emissivity of 0.5% is considered, errors between 0.3 K and 0.7 K are obtained. As has been shown in this example, the most important contribution corresponds to the atmospheric correction and the emissivity effect. Hence, at least an error on T_s between 0.3 K and 0.8 K is obtained, so it is difficult to retrieve the LST with an accuracy lower than these values unless accurate *in situ* values for emissivity and atmospheric parameters were available.

8. Conclusions

The LST retrieved by thermal infrared remote sensing techniques is one of the most used parameters for environmental studies. For this purpose, several algorithms can be used, as split-window or dual-channel, dual-angle, etc. These algorithms retrieve LST with a certain error, so they are obtained by an approximation to the radiative transfer equation, simulation procedures and statistical fits. However, the use of the radiative transfer equation itself does not guarantee an accurate value of LST, even if the atmospheric correction is free of errors. Only the uncertainty on the land surface emissivity leads to an error on the LST of 0.4 K, although this error is reduced to 0.2 K when *in situ* values are considered. The atmospheric correction introduces errors on the LST retrieval of 0.2 K or 0.7 K depending if *in situ* or remote sensing data are used, respectively. So, in optimal conditions and when *in situ* data are available, a minimum error of 0.3 K is obtained, whereas when remote sensing data are considered a minimum error of 0.8 K is expected. When other error sources such as noise error, bandpass effects and wavelength indetermination are considered, then an accuracy for the LST retrieval between 0.5 and 0.9 K is obtained.

Acknowledgments

We wish to thank the European Union (EAGLE, project SST3-CT-2003-502057) and the Ministerio de Ciencia y Tecnología (project REN2001-3105/CLI) for the financial support. This work has been carried out while Juan C. Jiménez was in receipt of a grant from the Universitat de València.

References

Abreu, L.W. and Anderson, G.P. (Eds), 1996, The MODTRAN 2/3 Report and LOWTRAN 7 MODEL, Modtran Report, Contract F19628-91-C-0132, Hanscom, MA: USA.

BARTON, I.J., 1992, Satellite-derived sea surface temperatures: a comparison between operational, theoretical and experimental algorithms. *Journal of Applied Meteorology*, **31**, pp. 432–442.

BECKER, F. and LI, Z.-L., 1990a, Temperature-independent spectral indices in thermal infrared bands. *Remote Sensing of Environment*, **32**, pp. 17–33.

BECKER, F. and LI, Z.-L., 1990b, Towards a local split-window method over land surfaces. *International Journal of Remote Sensing*, **11**, pp. 369–393.

BECKER, F. and LI, Z.-L., 1995, Surface temperature and emissivity at various scales: definition, measurement and related problems. *Remote Sensing Reviews*, **12**, pp. 225–253.

DASH, P., GÖTTSCHE, F.-M., OLESEN, F.-S. and FISCHER, H., 2002, Land surface temperature and emissivity estimation from passive sensor data: theory and practice—current trends. *International Journal of Remote Sensing*, **23**, pp. 2563–2594.

GILLESPIE, A.R., ROKUGAWA, S., HOOK, S., MATSUNAGA, T. and KAHLE, A.B., 1998, A temperature and emissivity separation algorithm for Advanced Spaceborne Thermal Emission and Reflection Radiometer (ASTER) images. *IEEE Transactions on Geoscience and Remote Sensing*, **36**, pp. 1113–1126.

JIMÉNEZ-MUÑOZ, J.C. and SOBRINO, J.A., 2003, A generalized single-channel method for retrieving land surface temperature from remote sensing data. *Journal of Geophysical Research*, **108**, doi: 10.1029/2003JD003480.

LAGOUARDE, J.P., KERR, Y.H. and BRUNET, Y., 1995, An experimental study of angular effects on surface temperature for various plant canopies and bare soils. *Agricultural and Forest Meteorology*, **77**, pp. 167–190.

LI, Z.-L. and BECKER, F., 1993, Feasibility of land surface temperature and emissivity determination from AVHRR data. *Remote Sensing of Environment*, **43**, pp. 67–85.

NERRY, F., LABED, J. and STOLL, M.P., 1998, Emissivity signatures in the thermal IR band for remote sensing: calibration procedure and method of measurement. *Applied Optics*, **27**, pp. 758–764.

PRATA, A.J., 1993, Land surface temperature derived from the Advanced Very High Resolution Radiometer and the Along-Track Scanning Radiometer 1. Theory. *Journal of Geophysical Research*, **98**, pp. 16 689–16 702.

PRATA, A.J., 1994, Land surface temperature derived from the Advanced Very High Resolution Radiometer and the Along-Track Scanning Radiometer 2. Experimental results and validation of AVHRR algorithms. *Journal of Geophysical Research*, **99**, pp. 13 025–13 058.

QIN, Z. and KARNIELI, A., 1999, Progress in the remote sensing of land surface temperature and ground emissivity using NOAA-AVHRR data. *International Journal of Remote Sensing*, **20**, pp. 2367–2393.

RICHTER, R. and COLL, C., 2002, Bandpass resampling effects for the retrieval of surface emissivity. *Applied Optics*, **41**, pp. 3523–3529.

SCHMUGGE, T., FRENCH, A., RITCHIE, J.C., RANGO, A. and PELGRUM, H., 2002, Temperature and emissivity separation from multispectral thermal infrared observations. *Remote Sensing of Environment*, **79**, pp. 189–198.

SCOTT, N.A. and CHEDIN, A., 1981, A fast line by line method for atmospheric absorption computations: the Authomatized Atmospheric Absorption Atlas. *Journal of Meteorology*, **20**, pp. 802–812.

SOBRINO, J.A. and CASELLES, V., 1993, A field method for measuring the thermal infrared emissivity. *ISPRS Journal of Photogrammetry and Remote Sensing*, **48**, pp. 24–31.

SOBRINO, J.A. and CUENCA, J., 1999, Angular variation of thermal infrared emissivity for some natural surfaces from experimental measurements. *Applied Optics*, **38**, pp. 3931–3936.

SOBRINO, J.A., CASELLES, V. and BECKER, F., 1990, Significance of the remotely sensed thermal infrared measurements obtained over a citrus orchard. *ISPRS Photogrammetric Engineering and Remote Sensing*, **44**, pp. 343–354.

SOBRINO, J.A., LI, Z.-L. and STOLL, M.P., 1993, Impact of the atmospheric transmittance and total water content in the algorithms for estimating satellite sea surface temperatures. *IEEE Transactions on Geoscience and Remote Sensing*, **31**, pp. 946–952.

SOBRINO, J.A., LI, Z.-L., STOLL, M.P. and BECKER, F., 1994, Improvements in the split-window technique for land surface temperature determination. *IEEE Transactions on Geoscience and Remote Sensing*, **32**, pp. 243–253.

SOBRINO, J.A., LI, Z.-L., STOLL, M.P. and BECKER, F., 1996, Multi-channel and multi-angle algorithms for estimating sea and land surface temperature with ATSR data. *International Journal of Remote Sensing*, **17**, pp. 2089–2114.

SOBRINO, J.A., JIMENEZ, J.C., RAISSOUNI, N. and SORIA, G., 2002, A simplified method for estimating the total water vapor content over sea surfaces using NOAA-AVHRR channels 4 and 5. *IEEE Transactions on Geoscience and Remote Sensing*, **40**, pp. 357–361.

WAN, Z. and LI, Z.-L., 1997, A physics-based algorithm for retrieving land-surface emissivity and temperature from EOS/MODIS data. *IEEE Transactions on Geoscience and Remote Sensing*, **35**, pp. 980–996.